Received: 18 May 2022 | Revised: 7 December 2022 | Accepted: 22 December 2022

DOI: 10.1111/jfr3.12882

ORIGINAL ARTICLE

CIWEM Chartered Institution of Water and Environmental Management | Journal of Flood Risk Management | WILEY

The effect of heterogeneities and small cavities on levee failures: The case study of the Panaro levee breach (Italy) on 6 December 2020

Francesca Ceccato | **Paolo Simonini**

Department of Civil Environmental and Architectural Engineering (DICEA), University of Padua, Padua, Italy

Correspondence
Francesca Ceccato, DICEA-University of Padua, via Ognissanti 39, 35129 Padua Italy.
Email: francesca.ceccato@dicea.unipd.it

Funding information
Ministero dell'Istruzione, dell'Università e della Ricerca, Grant/Award Number: 2017YPMBWJ; Ministry of Education, University and Research, Grant/Award Number: BIRD181859

Abstract

This article discusses the levee failure that occurred on 6 December 2020 at Castelfranco Emilia, near Modena (Italy), showing that it cannot be explained without assuming the presence of local heterogeneities or a small cavity. The possible presence of these defects is supported by evidence derived from historical data and site observations. Fully coupled hydromechanical finite element simulations prove that the river embankment assumed without any deficiency had a sufficient level of safety for the considered event, thus it is necessary to hypothesize the presence of a local defect. The presence of a small cavity, in hydraulic communication with the river and buried at shallow depth, is assumed. This could be, for example, a new den, an old animal burrow repaired only partially, or a rotten plant root. Numerical analysis shows that the increase in water pressure within the cavity can trigger local failure of the landside slope, thus starting concentrated erosion. In highly erodible soils, this mechanism can lead very rapidly to the opening of the breach. A new analytical expression for the factor of safety of the soil wedge between the cavity and the surface is proposed. This approach is very simple and easily applicable, for example, to the assessment of levee vulnerability to animal burrows at a large scale. The results of the study are relevant for the management of water retaining structures.

KEYWORDS

concentrated erosion, flood, levee breach, slope stability, small cavity

1 | INTRODUCTION

River levees and coastal dams are long structures that often have a very long history. Despite nowadays there are well-established design regulations and maintenance guidelines, for example, FEMA (2005), CIRIA (2013b), and national technical standards, in the past they were often built with a mixture of different materials, without following any design regulation, and without leaving any documentation on their features. In some cases, even improper encroachments, that is, structures not part of the levee's design, or excavations may have been created and then removed (CIRIA, 2013a). Furthermore, natural factors, such as weathering and biological activity, could

have altered the properties of the earth structures. For example, burrowing animals may dig holes or burrow tunnels and plant roots may decay leaving cavities. For these reasons, the stability of real earthen structures may be significantly affected by hidden local heterogeneities. These aspects are essential for the maintenance of flood defense system as discussed in CIRIA (2013a) and FEMA (2005).

Local defects may significantly reduce the stability of the earth structure by altering its structural and hydraulic integrity. The existence of a weak point may lead to a local collapse that can evolve into catastrophic failure; this could be, for example, an inclusion of low-strength material or even a cavity, such as those excavated by animals. The presence of a more permeable material, for example, fissures, plant roots, or animal burrows, may alter the pore pressure distribution in the soil, thus reducing its shear strength; in addition, it may create preferential flow paths that favor internal erosion mechanisms.

When there is a transverse crack or a pipe through the embankment, the water flow through the hole can generate concentrated erosion (Bonelli and Nicot, 2013). The cavity expands at a rate that depends on the erodibility of the material, the length of the path, and the pressure difference between the entrance and exit (Bonelli et al., 2007), and can rapidly lead to the opening of the breach if no countermeasures are taken (Camici et al., 2017; Orlandini et al., 2015). This phenomenon should not be confused with piping. Concentrated erosion occurs in a pre-existing cavity and it can be very fast, potentially leading to failure in a few hours (Bayoumi & Meguid, 2011; Bonelli et al., 2007; Savage et al., 2019); in contrast, piping is the formation of a pipe as a consequence of grain erosion due to seepage, and it usually progresses more slowly. Animal burrows and decayed plant roots may facilitate piping.

Although real levees and dams are heterogeneous structures, in standard practice, the stability is often studied assuming homogeneous materials with a cautious estimate of hydromechanical properties to evaluate a deterministic factor of safety (FS). More advanced analyses apply a probabilistic approach considering the uncertainty and spatial variability of soil properties and calculating a probability of failure (Pf) or a reliability index (Bonaccorsi et al., 2022; Bossi et al., 2016; Camici et al., 2017; Duncan, 2000; El-Ramly et al., 2002).

In the literature, the explicit consideration of local heterogeneities mainly focused on the study of crack formation in dams (He et al., 2021; Savage et al., 2019) and effect of animal burrows on levee stability. The latter has been recently investigated numerically and experimentally (Balistrocchi et al., 2021; Dassanayake and Mousa, 2020; Onda and Itakura, 1997; Palladino et al., 2020; Saghaee et al., 2017; Taccari, 2015).

There are several documented cases of levee and dam failures that cannot be explained without assuming the existence of a local defect such as an animal burrow or a crack (Bayoumi & Meguid, 2011; Camici et al., 2017; Marble, 2012; Orlandini et al., 2015; Saghaee et al., 2017; Savage et al., 2019). This article illustrates a recent case of levee failure that cannot be explained assuming the structure homogeneous and without defects. The considered case study refers to the breach that opened on 6 December 2020 at Castelfranco Emilia, near Modena (Italy; Section 2).

The levee stability is analyzed performing fully coupled flow-deformation finite element method (FEM) simulations (Section 3), in which soil–water interaction are simulated and changes in hydraulic conditions and soil displacement are considered at the same time. It is shown that the levee without defects has a sufficient level of safety with respect to the most typical failure mechanisms, thus it is necessary to assume the presence of a local defect, such as a small cavity buried at shallow depth and in hydraulic connection with the river. In this case, the pressure increasing inside the cavity may expulse the soil wedge between the cavity and the surface triggering concentrated erosion, which led very rapidly to the opening of the breach.

This is an innovative approach, indeed, in the literature, the global stability is customarily investigated decoupling water–soil skeleton interaction analysis, and performing firstly seepage analyses and then slope stability analyses using the method of slices (Dassanayake and Mousa, 2020; Orlandini et al., 2015; Taccari, 2015). Stability analyses consider ex ante circular failure surfaces crossing the levee and foundation subsoil and calculate FS with the previously calculated pore pressure distribution assuming rigid-plastic soil behavior. The decrease in FS (or increase of Pf) in the damaged levee is considered a proof of concept of the risk associated with the presence of cavities, but, in some cases, the assumed failure surface may not be representative of the real conditions. In many studies, for example, Balistrocchi et al. (2021), Palladino et al. (2020), Taccari (2015), failure is assumed to occur when the phreatic line reaches the landside slope surface. This is the necessary condition for the onset of erosion at the toe or through the levee body which usually progresses more slowly than concentrated erosion.

In Section 4, a simplified approach, based on the limit equilibrium method (LEM), is proposed to evaluate the stability of the soil wedge between the cavity and the surface. Parametric analyses with different slope inclinations, cavity location, hydraulic load, and material parameters are performed to determine the conditions for

which this mechanism is more likely. Finally, Section 5 discusses the results drawing general suggestions for levee maintenance and risk analyses.

2 | CASE STUDY

The Panaro river is one of the right tributaries of the Po river, the longest Italian river crossing the Padana Plain. This is one of the most industrialized and productive areas in the country and river flooding can cause severe economic losses. The Panaro River flows from South to North, it springs in the Appenins and ends in the Po river, with a total length of 148 km and a basin of 2300 km^2. Close to S. Anna village, a large water storage was recently created to laminate flood. This system can store up to 24 million of cubic meters of water and limit the discharge to 500 m^3/s. Figure 1 shows an overview of the area.

A breach suddenly opened in the municipality of Castelfranco Emilia, near Modena on 6 December 2020, around 6:00 a.m. The breach progressively enlarged during the same morning, reaching a length of 80 m and was effectively closed in less than 24 h. A volume between 7 and 9 million cubic meters of water inundated an area of about 15 km^2.

The breach opened in the early morning in a location relatively far from the inhabited areas, thus direct observations of the early stages of the phenomenon are missing. However, it is clear that the water level was much lower than the levee crest (about 1.5 m), as shown in Figure 2. Previous evaluations of the safety factor, as connected to overflowing and seepage in undisturbed levees, did not suggest significant risks at this location (Fiorentini, Moretti, & Orlandini, 2016). However, as reported above, this levee failed when river-flow was significantly less than the design limit as also occurred in 2014 along the Secchia and Panaro Rivers (Orlandini et al., 2015).

Determining the causes of the levee failure in December 2020 is not trivial and multiple concurrent causes must be considered, such as geomechanical characteristic of materials, levee geometry, possible occurrence of local structural deformities, and local damages due to natural or anthropogenic actions. As a first step, the location of the breach is inspected, then documentation is collected including historical data on previous failures in the area, cartographic information, and topographic survey (Section 2.1). Specific geotechnical investigations are carried out to draw a geotechnical model of the levee and its foundation (Section 2.2). Finally, the occurrence of different failure causes is evaluated with the support of FEM analyses (Section 3).

2.1 | Historical and field observations

A significant number of flood events have been recorded in the last centuries along the Panaro river, see the works by Carnevali (2017), Castaldini & Pellegrini (1989), Moratti & Pellegrini (1972), Panizza et al. (2004). In some cases, it has been attributed to overflow and internal erosion, but for most of the events the causes are unknown.

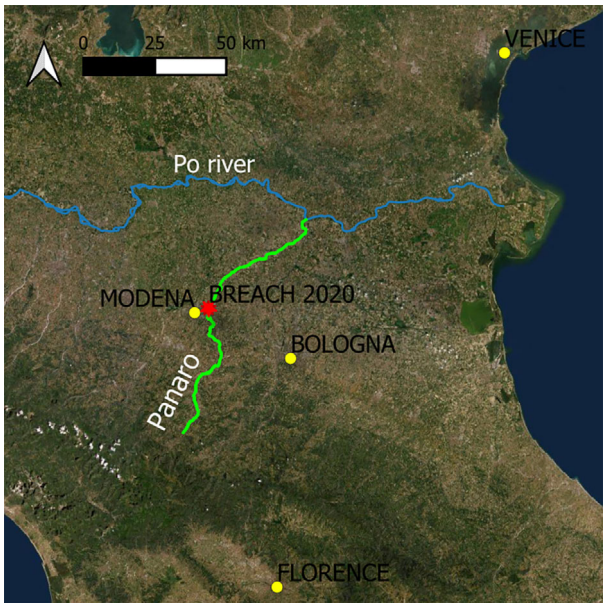

FIGURE 1 Overview of the area with location of the breach occurred on 6 December 2020 (Esri Satellite. 8 September 2022. https://server.arcgisonline.com/ArcGIS/rest/services/World_Imagery/MapServer/tile/{z}/{y}/{x}).

FIGURE 2 Photo of the breach at 8:40 on 6 December.

In the last decade, two erosion phenomena were observed very close to the new breach (Figure 3): (i) sand boils were observed in 2019 and kept under control with sandbags rings and (ii) concentrated erosion due to animal burrow was observed in 2014, leading to a 3 m settlement of the crest rapidly repaired preventing breach opening (Orlandini et al., 2015).

Near the location of the breach, two animal burrows were detected and repaired in 2016 by tamping backfill soil into the holes due to economic restrictions (Figure 3). However, the dens can be very long and with complex structures (Borgatti et al., 2017; Fischer and Dunand, 2016), therefore, complete repair of the cavity system using this method may be difficult and it is possible that part of the tunnel was still present. Despite the effort paid by the regional authority to control the population of burrowing animals, in recent years, their number has probably increased, as suggested by several sightings of badgers, foxes, porcupines, and nutria. Furthermore, five open burrows were detected a few days after the breach (Figure 3) and rapidly repaired.

Peculiar elements were found in the crevasse spillway, that is, 518 pieces of ancient bricks and concrete blocks dated back to the late 19th century (Figure 4) and rizhomes of Arundo Donax (giant cane; Figure 5). The relatively small amount of bricks suggests the possible presence of an old buried structure in the levee, but no documentation was found. Arundo Donax is a tall perennial cane belonging to reed species, it can grow in a variety of soils, but prefers wet-drained soils. Aerial photos confirmed the presence of this vegetation until 2012, then it was removed during maintenance works, but some of

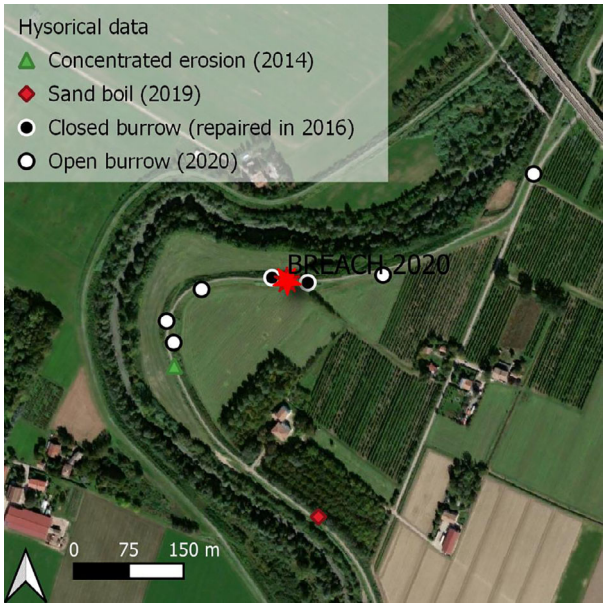

FIGURE 3 Historical and field observation near the breach (Google Satellite 8 September 2022. https://mt1.google.com/vt/lyrs=s&x={x}&y={y}&z={z})

FIGURE 5 Rhizomes of Adundo Donax found in the crevasse spillway.

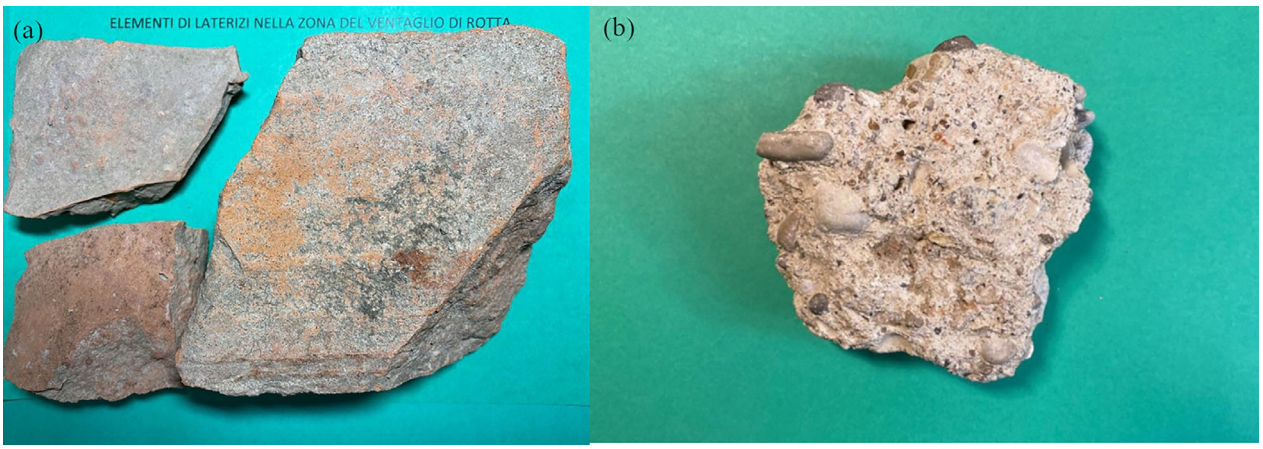

FIGURE 4 Material found in the crevasse spillway: (a) lateritic pieces and (b) concrete pieces dated 19th century

the rhizomes were still present and one could speculate that they could be partially rotten leaving a cavity.

This survey suggests that the levee system is relatively fragile, burrowing animals are active, and the embankments are easily subjected to internal erosion processes. Moreover, there is evidence supporting the hypothesis of the existence of local defects or even a small cavity that could have caused or facilitated the failure.

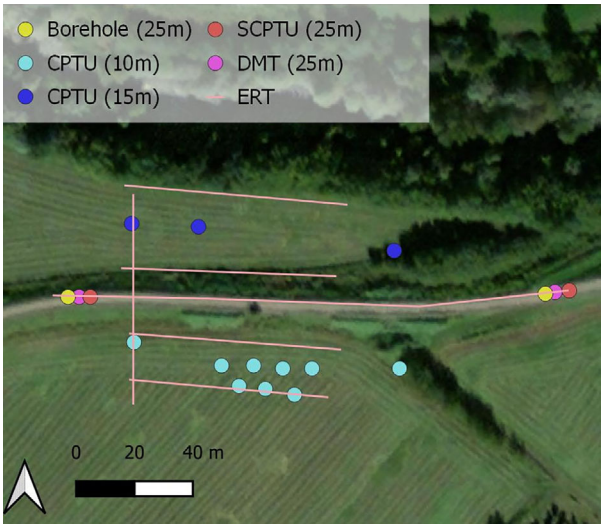

FIGURE 6 Site investigations (Google Satellite 8 September 2022. https://mt1.google.com/vt/lyrs=s&x={x}&y={y}&z={z})

2.2 | Site investigations and geotechnical model

The geotechnical campaign conducted in the area of the breach consisted in 12 piezocone penetration tests (CPTU), 2 seismic piezocone tests (SCPTU), 2 dilatometers (DMT), and 2 boreholes, 6 elettromagnetic survey (ERT) as shown in Figure 6. A total of 11 undisturbed samples were collected for laboratory testing. Laboratory tests included classification tests, direct shear tests, triaxial tests, permeability tests, and water retention tests. Penetration tests revealed that the top 2 m of the levee have a higher tip resistance, and this is probably a levee heightening realized with well-compacted sandy silt (Unit 1). The foundation of the levee is sandy silt and silty sand up to 15 m-depth where a clayey silt is found. Figure 7 shows the soil profile and Table 1 summarizes the geotechnical properties of the units estimated from the geotechnical survey.

The earth embankment is made of a mixture of sand and silt in different proportions, a small percentage of clay is found only in one sample. As shown in Table 2, sand content in Units 1 and 2 ranges between 23% and

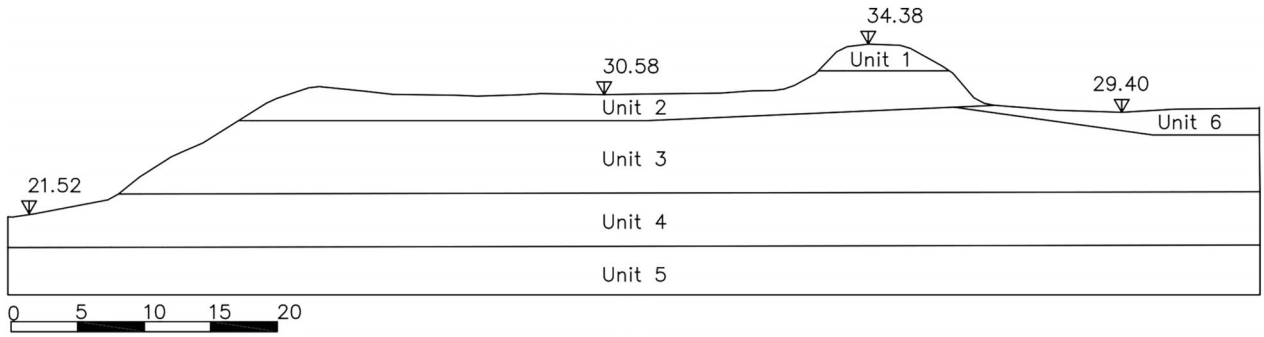

FIGURE 7 Geometry and stratigraphy of the levee (units are in meters, elevation is with respect to the m.s.l.).

TABLE 1 Geomechanical properties of the stratigraphic units (γ, unit weight; φ′, friction anlge, c', effective cohesion, c_u, undrained shear strength; k_{sat}, saturated hydraulic conductivity).

Unit	Description	γ (kN/m^3)	φ (°)	c' (kPa)	c_u (kPa)	k_{sat} (m/s)
1	Fine sand with silt, well compacted	18.5–19.0	34–38	2–12	n.p.	1E-07–5 E-06
2	Fine sand with silt	16.4–19.2	31–33	2–12	n.p.	1E-07–5 E-06
3	Silt and sandy silt	18.4–18.8	29–31	6–9	n.p.	5E-08–5 E-07
4	Sand and silty sand	17.5–18.5	30–34	0		2E-06–2 E-05
5	Clayey silt	18.5–19.5	—	n.p.	60–80	1E-09–1 E-08
6	Silt and clayey silt	17.5–18.5	—	n.p.	20–50	1E-09–4 E-08

TABLE 2 Granulometric properties, unit weight (γ) and degree of saturation (S) of the undisturbed samples.

Sample ID	Reference depth (m)	Unit	Sand (%)	Silt (%)	Clay (%)	γ (kN/m^3)	S (%)
S1-C1	1.25	1	27.7	72.3	0.0	18.5	43
S2-C1	1.25	1	49.2	50.8	0.0	18.8	59
S1-C2	2.75	2	64.2	30.2	5.6	16.4	19
S1-C3	4.25	2	34.6	65.4	0.0	—	—
S2-C2	2.75	2	58.2	41.8	0.0	16.7	54
S2-C3	4.25	2	22.8	69.6	7.6	19.2	79
S1-C4	6.75	3	51.4	40.0	8.6	18.4	52
S1-C5	9.25	3	73.3	26.7	0.0	18.7	88
S2-C4	6.75	3	20.1	65.9	14.0	18.8	81
S2-C5	9.25	3	41.7	58.3	0.0	15.5	56
S2-C6	12.25	4	91.3	8.7	0.0	17.5	82

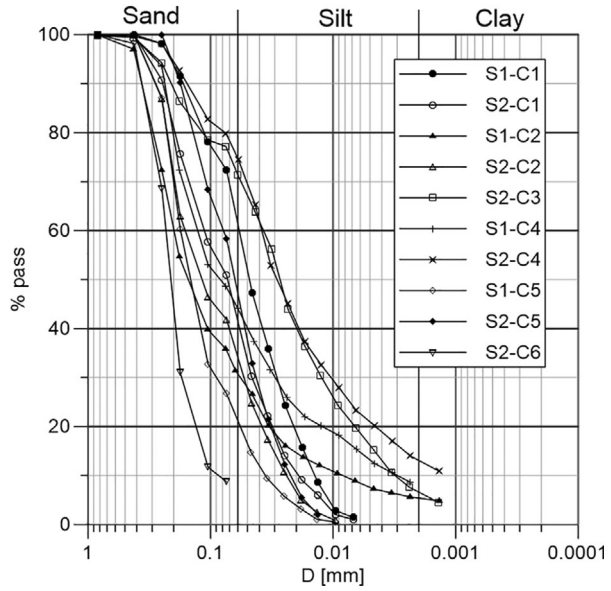

FIGURE 8 Granulometric curves, for undisturbed samples (see Table 2).

64% and silt content ranges between 30% and 72%; Figure 8 shows the grain size distributions. Natural unit weight varies between 16.4 and 19.2 kN/m^3 and the degree of saturation is between 20% and 80% with higher values for greater depths. Figure 9 shows the soil–water retention curves and the hydraulic conductivity curves; note that in unsaturated conditions the hydraulic conductivity of these materials is very low. Soil friction angle is between 34° and 38° for Unit 1 and between 31° and 33° for Unit 2. Cohesion varies in a wider range, between 0 and 12 kPa. This parameter is crucial in levee safety analyses because it can greatly modify the safety factor of shallow slip surfaces; however, it is not trivial to estimate because in unsaturated soils it depends on suction.

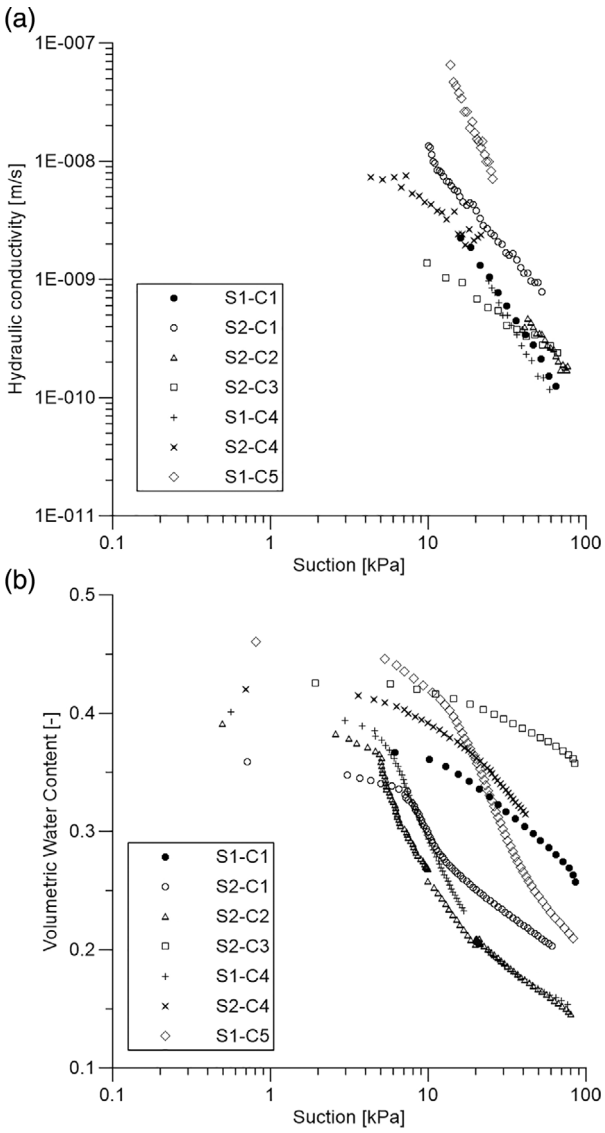

FIGURE 9 (a) Hydraulic conductivity curves and (b) soil–water retention curves, for undisturbed samples (see Table 2).

A LiDAR survey carried out before the breach showed that in this location the slope is relatively steep, between 35° and 50°, the levee is 5-m high, 16 m-wide at the base, and the crest width is between 2 and 3.5 m.

3 | ANALYSIS OF POSSIBLE FAILURE MECHANISMS

The failure mechanisms analyzed in this case study are (i) the macro-instability of the landside slope eventually involving also the foundation soil (Figure 10a), (ii) internal erosion in the foundation or in the levee body (backward erosion piping Figure 10b), and (iii) concentrated erosion at a pre-existing pipe (Figure 10c). Macroinstability is a global failure of the slope that, in this case, could have been triggered by the reduction of soil shear strength due to the increase of pore pressures during seepage. Backward erosion piping consists in the erosion of soil grains initially at the outer surface and the formation of a small pipe which can progress through or under the levee body, increasing its size and bringing the levee to failure. It is triggered when the saturation front reaches the outer surface and the local hydraulic gradient is larger than a critical hydraulic gradient. Piping manifests with sand boiling, it usually progresses relatively slowly and can be controlled with sandbags rings as occurred in 2019 (see Section 2.1 and Figure 3). Concentrated erosion occurs when there is a preferential flow path, such as a pipe or a crack, that connects the waterside and the landside. When the contact shear stress generated by the flow at the boundary of the conduct exceeds the critical soil shear stress, particles are eroded and the size of the pipe increases leading to failure. This mechanism can lead very rapidly to the opening of the breach.

In order to evaluate the possible occurrence of these mechanisms, finite element analyses followed by slope stability analyses are carried out, as detailed in the next sessions. Other typical levee failure mechanisms, such as overflow, overtopping, translational sliding, and macro instability of the waterside slope, are considered impossible in this case.

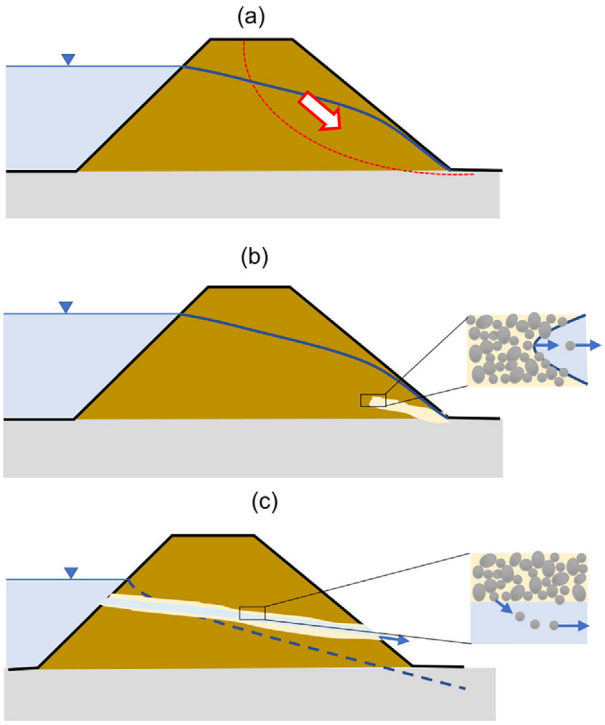

FIGURE 10 Possible failure mechanisms: (a) global stability of the slope, (b) backward erosion piping, and (c) concentrated erosion

3.1 | Methodology

Flow-deformation fully coupled analyses in transient conditions, followed by slope stability analyses, are performed with MIDAS GST NX (MIDAS IT Co., Ltd., 2020). In fully coupled analyses, changes in hydraulic conditions and soil displacements are considered at the same time, thus pore pressure changes influences soil displacements and vice versa; nodal pressures and displacements are the primary variables of the FEM formulation. Further details on the methodology can be found in the Appendix A and in the manual of the software. The advantage of a fully coupled FEM analysis is that the soil–water hydromechanically coupled interactions are considered in the governing equations and the (eventual) failure mechanism is a result of the simulation and not assumed ex ante as in the case of LEM with the method of slices often applied in practice.

The FS of the slope is calculated with the strength reduction method (SRM), which consists in the progressive weakening of the shear strength parameters of the soil until failure is reached (Griffiths and Lane, 1999). The final shear strength reduction factor corresponds to the FS.

Stratigraphy, discretization, and boundary conditions (BC) are shown in Figure 11. Material parameters are listed in Table 3. Partially saturated effects are accounted for Units 1, 2, 3, and 6, and the Van Genuchten (1980) function is used for the soil–water retention curve (Equation 1) and hydraulic conductivity curve (Equation 2):

$$\theta = \theta_{res} + \frac{\theta_{sat} - \theta_{res}}{(1 + (ah)^n)^m} \quad (1)$$

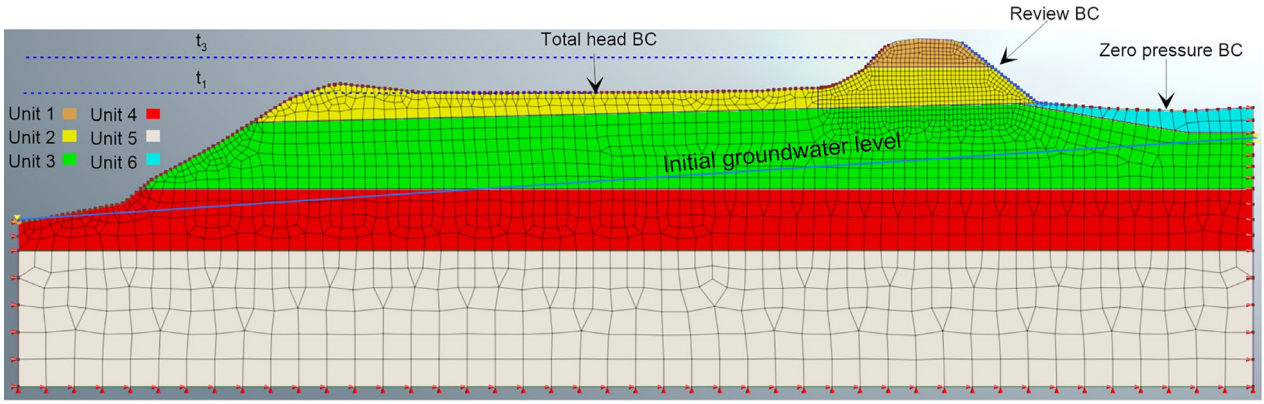

FIGURE 11 Discretization and boundary conditions of the numerical model.

Unit	γ (kN/m^3)	e_0	K_{sat} (m/s)	c (kPa)	φ (°)	E (kPa)	ν (–)
1	18.5	0.666	1.00 E-07	5	33	30,000	0.3
2	18	0.666	5.00 E-07	3	31	30,000	0.3
3	18.3	0.697	1.00 E-07	7	29.5	30,000	0.3
4	18	0.6	2.00 E-05	5	30	30,000	0.3
5	19	0.6	1.00 E-08	60	0	30,000	0.3
6	17.5	0.7	4.00 E-08	20	0	30,000	0.3

TABLE 3 Material parameters assumed for numerical analyses (γ, unit weight, e_0, initial void ratio, φ′, friction anlge, c, cohesion, E, Young modulus, ν, Poisson's ratio, k_{sat}, saturated hydraulic conductivity)

TABLE 4 Unsaturated material properties

Unit	θ_{res} (–)	θ_{sat} (–)	a (m^{-1})	n (–)	m (–)
1	0.094	0.40	0.337	1.43	0.300
2	0.133	0.40	2.085	1.947	0.486
3	0.168	0.41	0.523	2.245	0.554
6	0.100	0.41	0.500	1.5	0.333

$$\frac{k}{k_{sat}} = \frac{\left(1-(ah)^{n-1}\left(1+(ah)^{n}\right)^{-m}\right)^{2}}{\left(1+(ah)^{n}\right)^{\frac{m}{2}}} \quad (2)$$

where h is the matric suction head, θ, θ_{res}, and θ_{sat} is the volumetric water content, residual water content and saturated water content respectively, a, n, and m are material constants. The reference parameters are in Table 4.

The hydraulic head corresponding to the river hydrograph is applied at the nodes of the waterside (*total head BC*). The hydrograph is shown in Figure 12; it was derived from the measured hydrometric level at the closest measuring station. Water level reached the level of the floodplain in 11 h (t_1) and the breach opened after about 29 h, at time (t_3). Note that the reference system of the model is the mean sea water level. The landside slope is a potential seepage face; in Midas GTS NX this boundary condition is called *review BC* (Figure 10). Zero pressure is applied at the toe of the levee on the landside

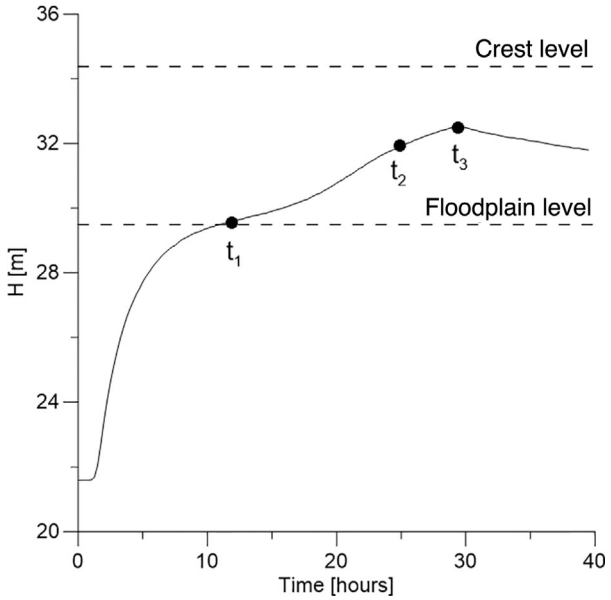

FIGURE 12 Hydrograph estimated at the breach section for the event of 6 December 2020.

because a water stagnant zone is hypothesized at this location, where the shallowest layer is formed mostly by a clayey soil and a small irrigation ditch gentle sloping toward the levee is observed. Note that this assumption accelerates material saturation, thus it represents a worst-case scenario.

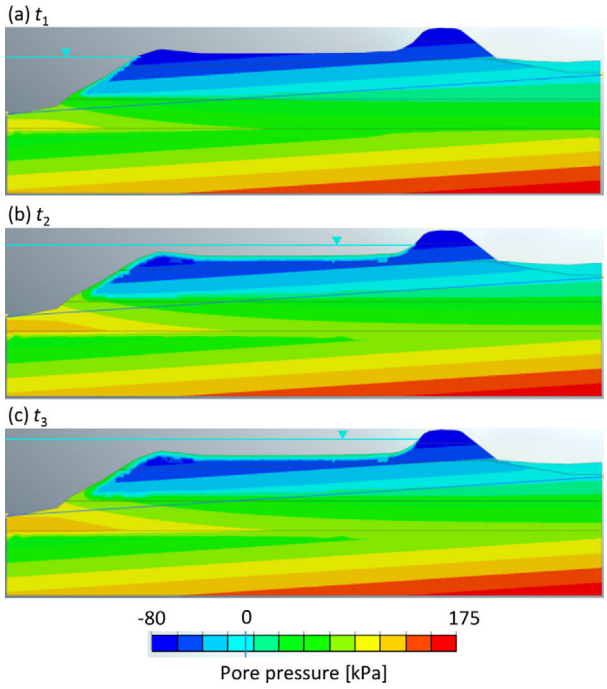

FIGURE 13 Pore pressure distribution at different time instants (negative pressures are matric suctions)

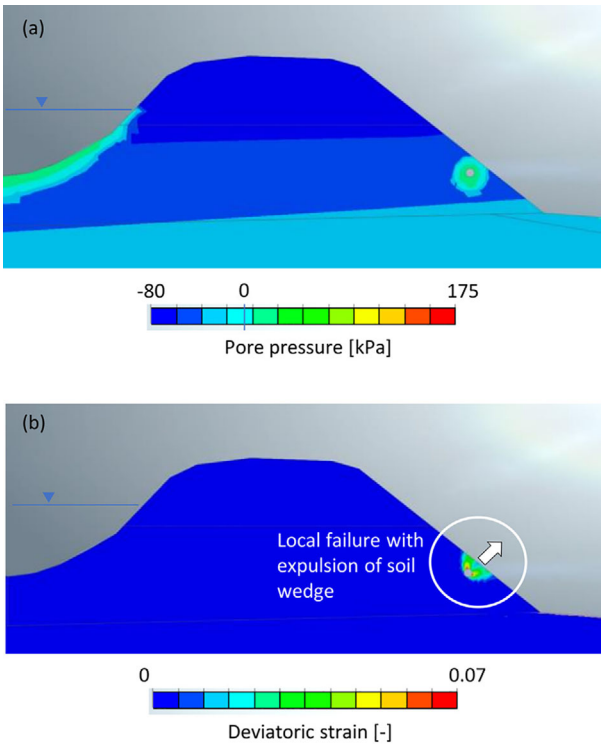

FIGURE 14 Model results for damaged levee: (a) pore pressure and (b) deviatoric strain at t_3

The initial depth of the water table on the landside is assumed to be 1 m. This is a conservative value, indeed during the field investigations carried out 1 month after the event, it was measured at 5 m depth.

First, the levee is assumed homogeneous and without defects (Section 3.2). Second, we assume the presence of a cavity, buried at a shallow depth, in which the pore pressure increases according to the river level (Section 3.3). This cavity could be, for example, a new animal den with the entrance on the riverside, part of an old burrow, or rotten plant roots.

3.2 | Results for undamaged levee

Figure 13 shows the pore pressure distribution at different time instants indicated in Figure 12. It can be noted that due to the low permeability of the unsaturated silty sand and the short duration of the flood, the wetting front does not penetrate significantly inside the levee body. Significant pore pressure changes occur only on the waterside slope, with limited consequences on the overall embankment stability. Indeed, the FS of the slope, calculated with SRM, is equal to 2.9 throughout the simulation. The embankment core tends to remain largely unaffected by changes in river water levels, due to its soil retention characteristics. This behavior is in agreement with monitoring data on similar embankments on the Secchia river (Rocchi et al., 2020).

These results show that macro instability is very unlikely because FS is significantly greater than one. The wetting front does not reach the outer surface; thus, piping cannot be triggered; furthermore, this internal erosion mechanism manifests with sand boils and usually progresses slowly, but this failure occurred very rapidly apparently without any sign. We can conclude that this levee, assumed homogeneous, should have been safe during the considered event and the observed failure can only be explained assuming the presence of a local defect.

3.3 | Results for damaged levee

To explain the observed failure, it is necessary to hypothesize the presence of a local defect. In this section, the presence of a small cavity near the landside slope in hydraulic communication with the river is assumed. The pressure inside the cavity increases as the water level increases and this has a double effect of (i) increasing the pressure load on the small soil cover and (ii) reducing the soil shear strength, that depends on the effective stress, by increasing the pore pressure in the vicinity of the cavity.

Figure 14 shows the pressures and deviatoric strains at t_3. Numerical convergence could not be achieved after this point, meaning that the levee is failing. The deviatoric strain highlights the development of two failure

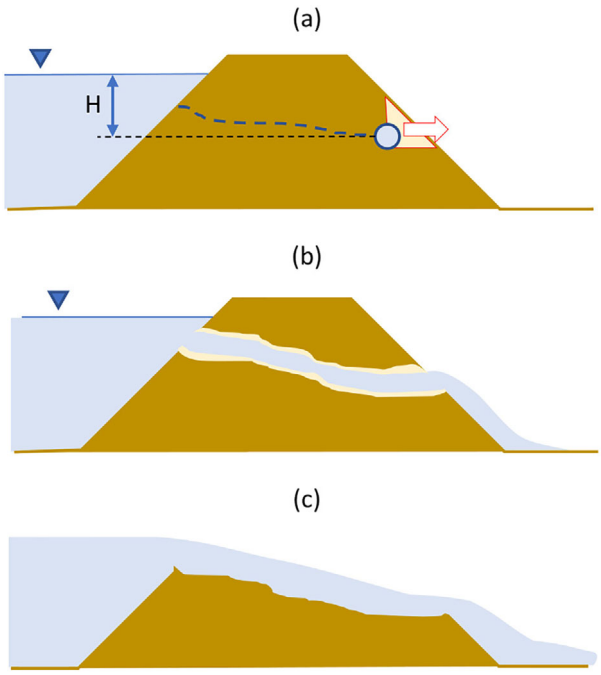

FIGURE 15 Hypothesized failure mechanism: (a) failure of the soil wedge, (b) progression of concentrated erosion, and (c) opening of the breach.

surfaces that depart from the boundary of the cavity to the slope surface; they delimit a soil wedge that is expulsed by the increasing pressure load inside the cavity. This superficial local failure can start a concentrated erosion leading very rapidly to the opening of the breach, as illustrated in Figure 15.

When the contact shear stress generated by the flow through the pipe exceeds the critical soil shear stress τ_c, particles are eroded and the size of the conduct increases leading to failure.

Considering a circular pipe, the temporal evolution of the cavity radius R is described by Equation 3 proposed by S. Bonelli et al. (2007)

$$\frac{R(\tilde{t})}{R_0} = \tilde{\tau}_c + (1-\tilde{\tau}_c)\exp(\tilde{t}) \tag{3}$$

where R_0, initial cavity radius; $\tilde{t} = t/t_{er}$, nondimensional time; $t_{er} = 2\rho_d L/k_{er}\Delta p$, characteristic time; $\rho_d \cong 1600\,\mathrm{kg/m^3}$, dry soil density; k_{er} erodibility coefficient; $\Delta p = H\gamma_w$, pressure difference between the entrance and the exit of the conduct; H, total head difference between entry and exit; $\gamma_w = 9.81\,kN/m^3$, unit weight of water. L, pipe length; $\tilde{\tau}_c = \tau_c/R_0\Delta p$, nondimensional critical shear stress; τ_c and k_{er} are material properties that can be estimated, for example, by hole erosion test. For silty sand, typical values of critical shear stress τ_c are between 8 kPa and 13 kPa, and typical erodibility coefficients k_{er} are between 0.001 and 0.014 m/s (Bonelli et al., 2007).

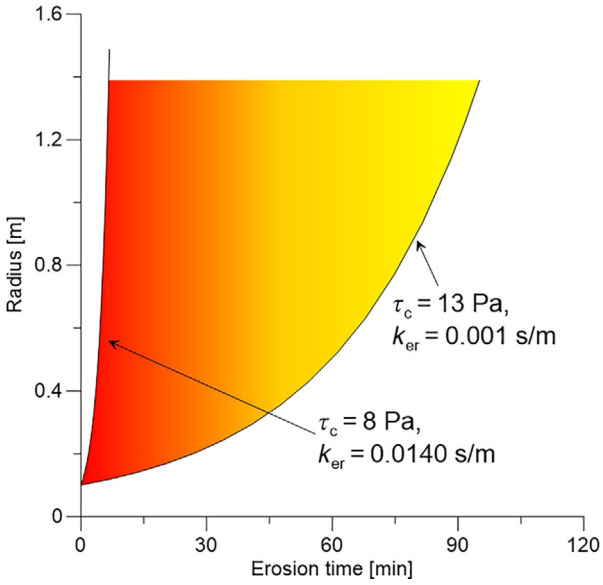

FIGURE 16 Evolution of cavity radius with time assuming different erosion parameters

Literature results show that silty sand and sandy silt are the materials with the lowest values of τ_c and the highest values of k_{er}; this means that the enlargement of the pipe progresses very rapidly (Bonelli et al., 2007).

Considering a pipe with the exit near the toe of the levee, it can be assumed $H = 1.6$ m, $L = 10$ m, $R_0 = 0.1$ m (typical of a small animal burrow). Figure 16 shows the evolution of the radius of the cavity over time. Under these assumptions, this mechanism can potentially lead to the opening of the breach in a few hours. This is compatible with the observation of a farmer living nearby who told that in the very early morning he did not notice any alarming signal and a few hours later the breach was already formed.

Direct field observations confirming the occurrence of this failure mechanism are not available, but it is compatible with the fast collapse observed and it is supported by the field and historical evidences described in Section 2.1. An animal burrow crossing transversally the levee could also explain such a rapid failure, but this eventuality is considered less probable because the length of animal burrows is proportional to their age and history (Roper, 2010) and these levees are periodically inspected and detected burrows are repaired.

4 | SIMPLIFIED 2D MECHANISM FOR THE STABILITY OF THE LANDSIDE SLOPE NEAR A CAVITY

As mentioned in Section 3, the most likely cause of failure is concentrated erosion possibly started by a local

failure of the landside slope due to pressure buildup inside a small cavity. This mechanism can explain the rapid opening of the breach. In this section, we illustrate a simple 2D model of local stability of the soil wedge between the cavity and the slope surface, consistent with the failure mode obtained in FEM (Figure 14). Although in reality the problem is more complex and 3D, we believe that the simplified model can provide and insight on the key features of the phenomenon.

We assume the presence of a cavity with diameter D located at a distance L_h from the outer slope, that is inclined at an angle β (Figure 17). This cavity is in communication with the river, thus the internal pressure increases with the hydraulic level ($p = \gamma_w H$), but no additional assumptions on the size and path are added. The Mohr-Coulomb failure criterion is used, and the soil shear strength parameters are φ and c. A 2D wedge stability is considered as shown in Figure 17, the base of the wedge is inclined of an angle α, which is assumed positive clockwise in Figure 17. If $\alpha > 0$, the FS can be expressed as Equation 4, where the wedge weight and the pressure load are unstabilizing forces as shown in Figure 17a.

$$FS^{+} = \frac{(W_{\perp} - U_{\perp})\tan\varphi + cL'}{U_{\parallel} + W_{\parallel}} \tag{4}$$

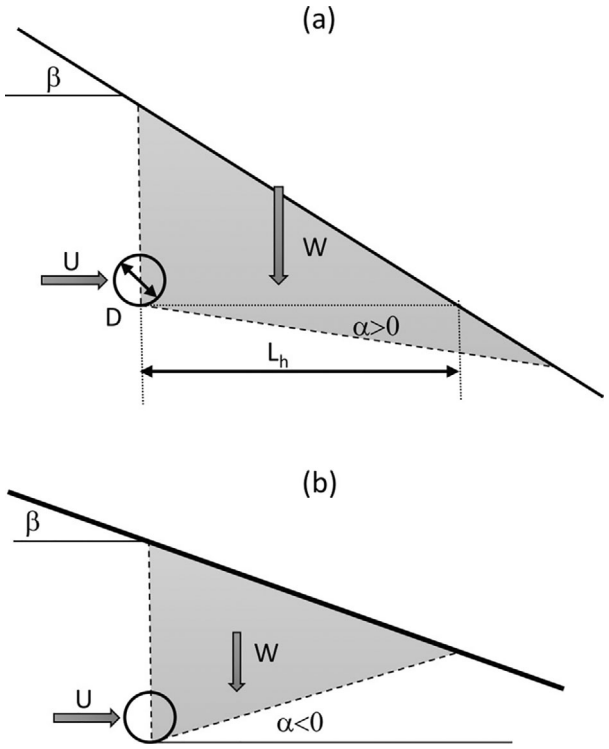

FIGURE 17 Simplified failure mechanism of the landside slope.

If $\alpha < 0$, FS is expressed by Equation (5) in which the wedge weight is a stabilizing component (Figure 17b).

$$FS^{-} = \frac{(W_{\perp} + U_{\perp})\tan\varphi + cL + W_{\parallel}}{U_{\parallel}} \tag{5}$$

For simplicity we assume $W = 0.5\gamma L_h^2 \tan^2\beta\cos\beta\cos\alpha/\sin(\beta-\alpha)$ and $U = D\gamma_w H$, the latter is horizontal.

$FS^{+/-}$ are a function of the inclination α of the failure surface. Figure 18 shows the FS as function of α for three different values of the slope angle β; the stars indicate the minimum FS. Note that for $\alpha = 0$, $FS^{+} = FS^{-}$. The slope inclination has a great influence on the failure mechanism, indeed for small values of β, FS^{-} tends to be lower than FS^{+}, the opposite is observed for large values of β.

A minimization procedure is implemented in MatLab to determine the angle θ_{min} providing the lowest FS. For given geometric parameters (L_h, D, β), hydraulic level (H) and material properties (φ, c), the FS is the minimum between Equation (4) and Equation (5), that is, $FS = \min(FS^{+}, FS^{-})$.

Figure 19 shows the effect of φ, c, β, and H on FS as function of L_h. As expected, the FS decreases with the increase of H (Figure 19a). For small values of L_h, FS decreases with the decrease of β and $\alpha_{min} < 0$ is usually observed; in contrast, for large values of L_h, FS decreases with the increase of β and $\alpha_{min} > 0$ is obtained. The friction angle has a limited impact, while the cohesion significantly modifies FS. Evaluating this parameter is not

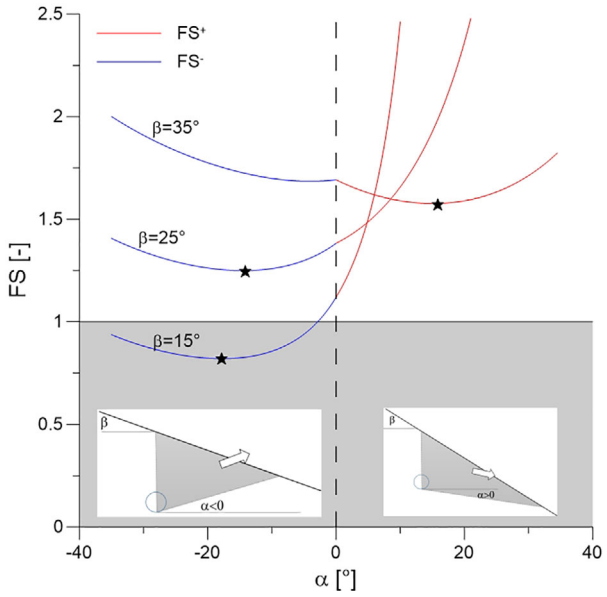

FIGURE 18 Factor of safety (FS) as function of inclination of failure surface for different slope inclinations ($H = 1.6$ m, $D = 0.25$ m, $L_h = 1$ m, $\gamma = 18$ kN/m^3, $c = 3$ kPa, and $\varphi = 30°$).

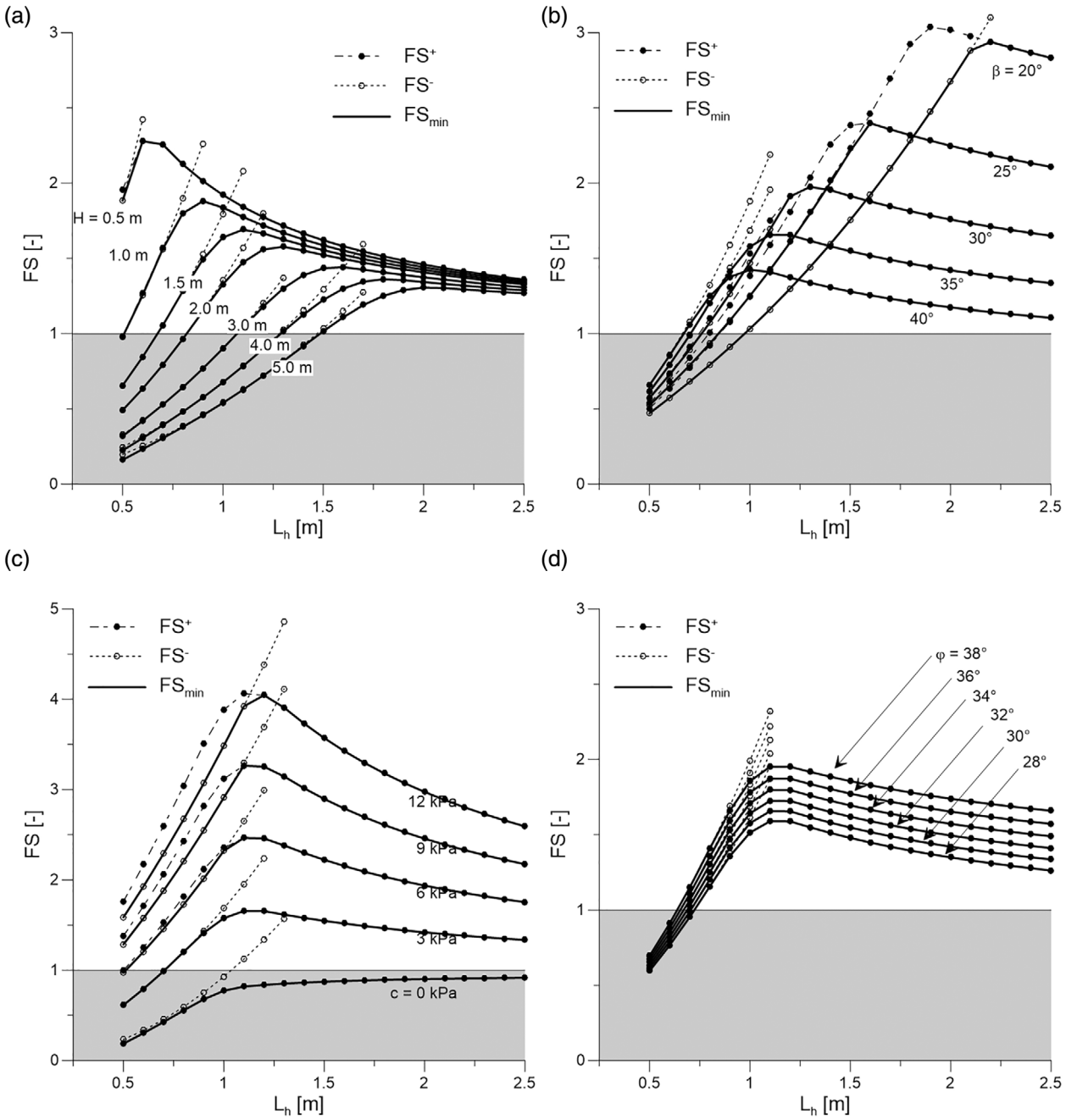

FIGURE 19 Factor of safety (FS) as function of L_h (if not otherwise specified $H = 1.6$ m, $D = 0.25$ m, $\gamma = 18$ kN/m^3, $c = 3$ kPa, $\varphi = 30°$, $\beta = 35°$): (a) effect of hydraulic head, (b) effect of slope inclination, (c) effect of cohesion, and (d) effect of friction angle.

trivial because, in partially saturated soils, apparent cohesion decreases when soil saturates (Fredlund et al., 1993; Vanapalli et al., 1996), this means that water infiltration decreases the strength parameters assumed for this analyses. Moreover, the superficial soil layer may be damaged by several anthropogenic and natural factors.

This approach is very simple and allows a quick estimate of FS or, by imposing FS = 1, a quick estimate of the critical geometrical parameters (L_h, D) and hydraulic load H (Ceccato et al., 2022). However, its range of validity is limited, indeed for small values of L_h, the simplified expressions used for W and U are not valid, while for large values of L_h, a circular failure of the slope is favored as discussed in (Dassanayake and Mousa, 2020).

Reasonable parameters for the considered case study are $H = 1.6$ m, $D = 0.25$ m, $\gamma = 18$ kN/m^3, $c = 3$ kPa, $\varphi = 31°$, and $\beta = 35°$, that provide FS = 1 for $L_h = 0.7$ m. This further supports the hypothesis that a cavity, buried at shallow depth, could be the cause of failure.

5 | DISCUSSION AND CONCLUSIONS

The levee failure of the 6 December 2020 at the Panaro River near Modena is presented in this work. Fully coupled numerical analyses using FEM showed that the levee assumed without defect had a significant margin of safety with the considered event; however, observations about historical failures occurred nearby and field observations suggested that local heterogeneities were present and they could have caused the failure. In particular, it is assumed that pressure buildup inside a small cavity below the slope surface caused a local instability that triggered concentrated erosion. In sand and silt mixtures, concentrated erosion progresses very rapidly, leading to the opening of the breach in a short time. This small cavity could represent, for example, a deteriorated plant root, a new den, an old animal burrow closed only partially. FEMA (2005) recommends to repair animal burrows by completely filling the cavity with slurry; however, sometimes filling of the hole by soil tamping is operated due to cost restrictions. Although this procedure is quick and economically affordable, it should be discouraged because it is possible that part of the tunnel remains open.

A new simplified method is proposed to evaluate the equilibrium of a wedge of soil between the cavity and the slope surface of the slope. The key parameters of the model are the slope angle, the depth of the cavity, the hydraulic head, and the shear strength parameters. The method has the advantage of being very simple and computationally inexpensive; thus, it is well applicable to probabilistic approaches to enrich the assessment of levee vulnerability to burrowing animals at large scale.

Future developments of the study should confirm experimentally the occurrence of this failure mechanism, consider 3D conditions, and fully coupled hydromechanical behavior of soil.

ACKNOWLEDGMENTS

Financial support from University of Padua (BIRD181859) and Italian Ministry of Education, University and Research (MIUR), Redreef - PRIN 2017 Call, prot. 2017YPMBWJ, are gratefully acknowledged.

DATA AVAILABILITY STATEMENT

The data that support the findings of this study are available from the corresponding author upon reasonable request.

ORCID

Francesca Ceccato https://orcid.org/0000-0002-8624-2179

REFERENCES

Balistrocchi, M., Moretti, G., Ranzi, R., & Orlandini, S. (2021). Failure probability analysis of levees affected by mammal bioerosion. *Water Resources Research*, *57*(12), 1–24. https://doi.org/10.1029/2021WR030559

Bayoumi, A., & Meguid, M. A. (2011). Wildlife and safety of earthen structures: A review. *Journal of Failure Analysis and Prevention*, *11*(4), 295–319. https://doi.org/10.1007/s11668-011-9439-y

Biot, M. A. (1941). General theory of three-dimensional consolidation. *Journal of Applied Physics*, *12*(2), 155–164. https://doi.org/10.1063/1.1712886

Bonaccorsi, B., Moramarco, T., Noto, L. V., & Barbetta, S. (2022). A multilayer soil approach for seepage process analysis in earthen levees. *Journal of Flood Risk Management*, *15*(3), e12801. https://doi.org/10.1111/jfr3.12801

Bonelli, S., Brivois, O., & Lachouette, D. (2007). The scaling law of piping erosion. 18ème Congrès Français de Mécanique, 18ème Congrès Français de Mécanique Grenoble, 27–31 Août 2007, 1–6.

Bonelli, S., & Nicot, F. (2013). Erosion in geomechanics applied to dams and levees. In *Erosion in geomechanics applied to dams and levees*. ISTE Ltd and John Wiley & Sons, Inc. https://doi.org/10.1002/9781118577165

Borgatti, L., Forte, E., Mocnik, A., Zambrini, R., Cervi, F., Martinucci, D., Pellegrini, F., Pillon, S., Prizzon, A., & Zamariolo, A. (2017). Detection and characterization of animal burrows within river embankments by means of coupled remote sensing and geophysical techniques: Lessons from river Panaro (northern Italy). *Engineering Geology*, *226*(May), 277–289. https://doi.org/10.1016/j.enggeo.2017.06.017

Bossi, G., Borgatti, L., Gottardi, G., & Marcato, G. (2016). The Boolean stochastic generation method - BoSG: A tool for the analysis of the error associated with the simplification of the stratigraphy in geotechnical models. *Engineering Geology*, *203*, 99–106. https://doi.org/10.1016/j.enggeo.2015.08.003

Camici, S., Barbetta, S., & Moramarco, T. (2017). Levee body vulnerability to seepage: The case study of the levee failure along the Foenna stream on 1 January 2006 (Central Italy). *Journal of Flood Risk Management*, *10*(3), 314–325. https://doi.org/10.1111/jfr3.12137

Carnevali, E. (2017). *La pericolosità alluvionale del Fiume Panaro nel tratto a nord di Modena (Emilia-Romagna)*. Università degli studi di Padova.

Castaldini, D., & Pellegrini, M. (1989). A review of the flow regulation system on the Secchia and Panaro rivers (Modena area, Italy). *Supplements of Geografiagch Fisica e Dinamica Quaternaria*, *ii*, 35–39.

Ceccato, F., Malvestio, S., & Simonini, P. (2022). Effect of animal burrows on the vulnerability of levees to concentrated erosion. *Water (Switzerland)*, *14*(18), 2777. https://doi.org/10.3390/w14182777

CIRIA (2013a). Operation and maintenance. In *The international levee handbook* (pp. 180–284). CIRIA. https://doi.org/10.13052/dgaej2156-3306.1635

CIRIA. (2013b). *The international levee handbook. C731*. CIRIA.

Dassanayake, S. M., & Mousa, A. (2020). Probabilistic stability evaluation for wildlife-damaged earth dams: A Bayesian approach. *Georisk*, *14*(1), 41–55. https://doi.org/10.1080/17499518.2018.1542499

Duncan, J. M. (2000). Factors of safety and reliability in geotechnical engineering. *Journal of Geotechnical Engineering*, *126*(4), 307–316.

El-Ramly, H., Morgenstern, N. R., & Cruden, D. M. (2002). Probabilistic slope stability analysis for practice. *Canadian Geotechnical Journal*, *39*(3), 665–683. https://doi.org/10.1139/t02-034

FEMA. (2005). *Dam Owner's guide to animal impacts on earthen dams (FEMA L-264)*. FEMA.

Fiorentini, M., Moretti, G., & Orlandini, S. (2016). Relazione tecnica sulla verifica funzionale delle arginature del fiume panaro.

Fischer, C., & Dunand, F. (2016). 3D topography and structure analysis of three European badger (Meles meles) setts from western Switzerland. *Wildlife Biology in Practice*, *12*(3), 26–35. https://doi.org/10.2461/wbp.2016.eb.3

Fredlund, D., Rahardjo, H., & Rahardjo, H. (1993). Soil mechanics for unsaturated soils. https://books.google.it/books?hl=it&lr=&id=ltVtPOGuJJwC&oi=fnd&pg=PA1&dq=Soil+Mechanics+for+Unsaturated+Soils+Author(s):++•%09D.+G.+Fredlund+B.Sc.,+M.Sc.,+Ph.D.,+•%09Dr.+H.+Rahardjo+civil+engineering,+M.Sc.,+Ph.D.,+First+published:17+Augus

Griffiths, D. V., & Lane, P. A. (1999). Slope stability analysis by finite elements. *Géotechnique*, *49*(3), 387–403. https://doi.org/10.1680/geot.1999.49.3.387

He, K., Song, C., & Fell, R. (2021). Numerical modelling of transverse cracking in embankment dams. *Computers and Geotechnics*, *132*(2020), 104028. https://doi.org/10.1016/j.compgeo.2021.104028

Marble, D. (2012). Santa Clara Dam Failure Memorandum to State Engineer Kent Jones. https://damfailures.org/wpcontent/%0Auploads/2022/01/Utah-Dam-Safety-Failure-Memo-Clean-Copy.pdf

MIDAS IT Co., Ltd. (2020). *Midas GTS NX* (2020 v1.1). http://www.midasuser.com/

Moratti, L., & Pellegrini, M. (1972). Caratteristiche delle alluvioni e dei dissesti verificatisi nei bacini dei fiumi Secchia e Panaro (provincie di Modena e Reggio Emilia) nel settembre 1972. *Atti della Societa dei Naturalisti e Matematici di Modena*, 183–195.

Onda, Y., & Itakura, N. (1997). An experimental study on the burrowing activity of river crabs on subsurface water movement and piping erosion. *Geomorphology*, *20*(3–4), 279–288. https://doi.org/10.1016/s0169-555x(97)00029-9

Orlandini, S., Moretti, G., & Albertson, J. D. (2015). Evidence of an emerging levee failure mechanism causing disastrous floods in Italy. *Water Resources Research*, *51*, 7995–8011. https://doi.org/10.1002/2015WR017426

Palladino, M. R., Barbetta, S., Camici, S., Claps, P., & Moramarco, T. (2020). Impact of animal burrows on earthen levee body vulnerability to seepage. *Journal of Flood Risk Management*, *13*(S1), 1–21. https://doi.org/10.1111/jfr3.12559

Panizza, M., Castaldini, D., Pellegrini, M., Giusti, C., & Piacentini, D. (2004). *Matrici geo-ambientali e sviluppo insediativo: un'ipotesi di ricerca* (pp. 31–62). Per Un Atlante Storico Ambientale Urbano.

Richards, L. A. (1931). Capillary conduction of liquids in porous mediums. *Physics*, *1*(5), 318–333.

Rocchi, I., Gragnano, C. G., Govoni, L., Bittelli, M., & Gottardi, G. (2020). Assessing the performance of a versatile and affordable geotechnical monitoring system for river embankments. *Physics and Chemistry of the Earth*, *117*(2018), 102872. https://doi.org/10.1016/j.pce.2020.102872

Roper, T. (2010). *Badger (Collins New Naturalist Library, Book 114)*. Harper Collins.

Saghaee, G., Mousa, A. A., & Meguid, M. A. (2017). Plausible failure mechanisms of wildlife-damaged earth levees: Insights from centrifuge modeling and numerical analysis. *Canadian Geotechnical Journal*, *54*(10), 1496–1508. https://doi.org/10.1139/cgj-2016-0484

Savage, S., Douglas, K., Fell, R., Peirson, W., & Berndt, R. (2019). Modeling the erosion and swelling of the sides of transverse cracks in embankment dams. *Journal of Geotechnical and Geoenvironmental Engineering*, *145*(5), 04019015. https://doi.org/10.1061/(asce)gt.1943-5606.0002040

Taccari, M. L. (2015). *Study upon the possible influence of animal burrows on the failure of the levee of san Matteo along the Secchia river*. Delft University of Technology.

Van Genuchten, M. (1980). A closed-form equation for predicting the hydraulic conductivity of unsaturated soils. *Soil Science Society of America Journal*, *44*(5), 892–898.

Vanapalli, S. K., Fredlund, D. G., Pufahl, D. E., & Clifton, A. W. (1996). Model for the prediction of shear strength with respect to soil suction. *Canadian Geotechnical Journal*, *33*(3), 379–392. https://doi.org/10.1139/t96-060

Zienkiewicz, O. C., Chan, A. H. C., Pastor, M., Schrefler, B. A., & Shiomi, T. (1999). *Computational geomechanics*. Wiley Chichester.

How to cite this article: Ceccato, F., & Simonini, P. (2023). The effect of heterogeneities and small cavities on levee failures: The case study of the Panaro levee breach (Italy) on 6 December 2020. *Journal of Flood Risk Management*, e12882. https://doi.org/10.1111/jfr3.12882

APPENDIX A

This appendix summarizes the governing equations of the fully coupled flow-deformation analysis implemented in the finite element software used in this study. Further details can be found in (Biot, 1941; MIDAS IT Co., Ltd., 2020; Zienkiewicz et al., 1999).

The following key definitions are introduced. The porosity n is the volume of voids to the total volume; the degree of saturation S is the ratio of free water to void volume and the volumetric water content is $\theta = nS$. The density of the soil–water mixture is $\rho = (1-n)\rho_s + nS\rho_w$ where ρ_s is the density of solid grains and ρ_w is the water density. Bishop's effective stress is used assuming the degree of saturation as an effective stress parameter:

$$\boldsymbol{\sigma} = \boldsymbol{\sigma}' + Sp_w\boldsymbol{m} \tag{A1}$$

Where $\boldsymbol{\sigma} = \left(\sigma_{xx}\,\sigma_{yy}\,\sigma_{zz}\,\tau_{xy}\,\tau_{yz}\,\tau_{zx}\right)^T$ is the vector of total stress, $\boldsymbol{\sigma}'$ is the effective stress, p_w is the pore pressure and $m = (1\,1\,1\,0\,0\,0)^T$. Note that compressive stresses and pressure are considered negative, thus suctions are positive pressures and air pressure is assumed to be zero. The hydraulic conductivity k in unsaturated conditions is a function of suction and it can be written as a fraction of the saturated hydraulic conductivity $k = k_{rel}k_{sat}$.

The governing equations are derived introducing the Darcy's law in the mass balance equation of (compressible) water (Equation A2) and the momentum balance equation of the mixture for static conditions (Equation A3):

$$\nabla^T\left[\frac{k}{g}\nabla p_w + \rho_w k\boldsymbol{g}\right] = -\frac{\partial(\rho_w nS)}{\partial t} \tag{A2}$$

$$\boldsymbol{\sigma} + \boldsymbol{g} = 0 \tag{A3}$$

where $\nabla^T = (\partial/\partial x, \partial/\partial y, \partial/\partial z)$ is the gradient operator, and $\mathbf{g}$ is the gravity vector, which has a length $g = 9.81\ m/s^2$.

The term on the right-hand-side of Equation (A2) can be written as

$$\frac{\partial(\rho_w nS)}{\partial t} = nS\frac{\partial\rho_w}{\partial t} + \rho_w n\frac{\partial S}{\partial t} + \rho_w S\frac{\partial n}{\partial t} \tag{A4}$$

In Equation (A4), $(\partial\rho_w)/\partial t = -(\rho_w/K_w)\,(\partial p_w/\partial t)$ represents the change in water density and K_w is the bulk modulus of water, $\partial t = (\partial S/\partial p_w)\,(\partial p_w/\partial t)$ is the change in degree of saturation and $\partial S/\partial p_w$ can be calculated from the soil–water retention curve, $\partial n/\partial t$ represents the compressibility of the soil. Note that neglecting the effect of soli compressibility in the flow equation, that is, $\rho_w S(\partial n/\partial t) = 0$, lead to the well known Richards equation of seepage problems in unsaturated porous media (Richards, 1931).

The discretized equations are derived from Equations (A2) and (A3) by applying the Galerking approach and introducing the finite element discretization technique. The BC are (nodal) soil displacements, loads, (nodal) water pressures or total heads and fluxes. The *review BC* can be applied at the interface with atmosphere if it is potential seepage, that is, water can flow out of the system at zero pressure but cannot enter the system in unsaturated conditions. With this condition the solver automatically switch from zero-flux BC to zero-pressure BC if necessary. Time integration applies a first order finite difference method and it is fully implicit. For nonlinear materials like soils the system of equations solved iteratively with the strategies typical of non-linear finite element solvers.